Identifying and quantifying point defects in semiconductors using x-ray-absorption spectroscopy: Si-doped GaAs

S. Schuppler,* D. L. Adler,† L. N. Pfeiffer, K. W. West, E. E. Chaban, and P. H. Citrin
AT&T Bell Laboratories, Murray Hill, New Jersey 07974
(Received 17 November 1994)

Both the type and concentration of point defects responsible for the observed poor electrical activity of highly Si-doped GaAs have been determined using near-edge and extended x-ray-absorption fine structure (NEXAFS and EXAFS). The measurements were made possible using a combination of synchrotron beamline features, fluorescence detection, and GaAs(311)*A* samples. Because Si can occupy both *n*-type Ga and *p*-type As sites, the electrical deactivation has generally been attributed to acceptor-Si atoms trapping free-electron carriers. However, the present NEXAFS data directly measure upper limts on the concentration of Si atoms occupying such *p*-type As sites, showing that only about half of the observed electrical inactivity is due to this autocompensation mechanism. Identification of the dominant defects responsible for the additionally missing carriers is provided by the EXAFS data, which reveal a comparatively large number of neutral Si_{Ga}-Si_{As} dimers and small Si_n clusters. Implications of these findings and a comparison with local vibrational mode spectroscopy and scanning tunneling microscopy methods are discussed.

I. INTRODUCTION

Gallium arsenide is the second-most used material in the semiconductor industry. Its direct band gap and high electron mobility lead to many different applications where speed and visible or ir light are involved, e.g., fast digital circuits and laser diodes. Despite this utility, some still believe that ". . .GaAs is the semiconductor of the future, and will always remain so."[1] Certainly the relative cost compared with Si-based technology is a dominant factor contributing to this view. However, another important factor is the degraded electrical activity of GaAs at high dopant concentrations. The goal of the present work is to investigate this phenomenon on a microscopic, atomistic level through direct experimental measurements.

The problem of electrical deactivation is encountered in all semiconductors, but it is particularly severe in GaAs doped by Si, its most common *n*-type dopant. As the Si doping level increases above a critical concentration of $\sim 5\times 10^{18}$ cm^{-3}, the number of free carries first saturates and then begins to drop off further with higher doping. By contrast, *n*-doped Si, as a host, typically saturates at $\lesssim 10^{21}$ cm^{-3} carriers and shows no additional reduction. This dramatic electrical deactivation in GaAs was recognized[2] only a few years after the discovery that III-V compounds were semiconducting.[3] A simple explanation for the deactivation, proposed as early as 1960,[4] has since been widely accepted: At low doping concentrations, Si atoms substitutionally occupy Ga sites in the host lattice, Si_{Ga}, and act as donors, but at higher concentrations the Si atoms begin to occupy As sites, Si_{As}, and act as acceptors. Thus the free carriers provided by Si donor atoms become trapped, or compensated, by other Si atoms acting as acceptors, in a process called autocompensation.[5]

The autocompensation mechanism appears to be plausible, but its importance has remained undetermined for more than 30 years. The reason for this was not due to lack of interest, but rather to a lack of experimental means for identifying and quantifying such dilute concentrations of atoms in such similar structural environments. For example, local vibrational model (LVM) spectroscopy, which probes defect-induced modes lying higher in energy than the maximum phonon energy of the host lattice, has been successful in identifying defect structures in semiconductor-impurity systems.[6] However, because some defects are sensitive to the electron bombardment treatment of the sample needed to detect these modes and because calibrating the oscillator strengths of the modes is not straightforward,[7] it is difficult to quantify the relative amounts of the defects using this spectroscopy. Other techniques capable of providing microscopic structural information from defects/dopants in semiconductors are therefore clearly desirable.

Given the historical interest in, the difficult nature of, and the obvious need for new methods to study this problem, it was understandably surprising when three independent groups recently published papers on the subject.[8–10] Two of the papers reported the identification of acceptor Be or Zn atoms[8] and of donor Si atoms[9] in GaAs using cross-sectional scanning tunneling microscopy (XSTM). The inherent sensitivity of STM to surface-related phenomena was overcome in those studies by cleaving the *n*- or *p*-type GaAs crystals *in vacuo* and probing up to five layers deep into the bulklike region of the sample edges. The third paper reported the identification of both Si_{Ga} and Si_{As} sites in the same sample as a function of dopant concentration using x-ray-absorption spectroscopy.[10] Improvements in measurement sensitivity enabled the bulk region of as-prepared samples to be probed, and from the relative amounts of Si_{Ga} and Si_{As} sites the autocompensation mechanism was shown to explain only about half of the observed deac-

0163-1829/95/51(16)/10527(12)/$06.00

tivation.

In the present work, we expand upon these earlier findings[10] and show how x-ray-absorption spectroscopy can be used to identify other species which contribute to the electrical deactivation of highly Si-doped GaAs. The role of Si dimers and clusters, in particular, is discussed. Another, more general, objective is to demonstrate the utility of this microscopic approach for characterizing and evaluating the importance of point defects specifically associated with dopants. Comparisons between capabilities and limitations of x-ray-absorption spectroscopy and those of XSTM and LVM spectroscopy are also presented.

II. EXPERIMENT

A. General background of EXAFS and NEXAFS

The well-established technique of extended x-ray-absorption fine-structure (EXAFS) for obtaining geometric structure[11] is based on the modulation of the photoabsorption cross section as a function of photon energy. The modulation, or fine structure, typically extends hundreds of electron volts above the absorption edge and arises from the interference between outgoing energetic core-excited photoelectron waves and those waves that have been backscattered from the core-dominated potentials of neighboring atoms. Short-range structural information, such as the distance and coordination number of atoms located $\lesssim 5$ Å around the absorbing atom, is obtained from the respective frequency and amplitude of the oscillatory EXAFS from a given coordination shell. Additional information, such as the identity of the neighboring atom(s) in that shell and the concentration of absorbing atoms in a given material, is contained in the respective shape of the EXAFS amplitude function and the amount of atomic absorption above and below the edge, i.e., the so-called edge jump. Analysis of EXAFS data is straightfoward because essentially only single scattering from chemically insensitive core potentials is involved. Moreover, the analysis is theory independent, relying instead on other EXAFS data from model systems of known structure containing the same or similar absorbing and backscattering atoms.

The region within about 50 eV from the absorption edge also contains structure, but of a very different kind. Here, low-energy photoexcited electrons scatter multiply off valence-dominated potentials, leading to structures sometimes larger than the edge jump itself. Because this near-edge x-ray-absorption fine structure, or NEXAFS [also referred to as x-ray-absorption near-edge structure (XANES) (Ref. 12)], *is* sensitive to electronic/chemical information, it can be thought of as N(ot)-EXAFS.[13]

Conventional EXAFS experiments, performed about twenty years ago with laboratory x-ray sources, measured absorption from bulk samples ($\sim 10^{22}$ atoms cm^{-3}) by detecting transmitted signals through thin films ($\lesssim 10$ μm). Present day synchrotron radiation sources with $> 10^5$ intensity enhancements have reduced these earlier EXAFS measurement times from weeks to minutes and have enabled the study of increasingly dilute materials. In such systems, EXAFS is measured not by transmission (the signal-to-background ratio would be too low) but by monitoring the radiative or nonradiative byproducts of the absorption process, namely, the fluorescent photons or the Auger (or secondary) electrons. The choice of detection scheme is governed largely[12,14] by the desired sampling depth. Thus, the short escape lengths of Auger electrons (< 100 Å) make that detection scheme more appropriate for surface-related systems, while fluorescence detection is more suitable for measuring absorption from atoms in the bulk.

Improvements in x-ray intensities and detection capabilities have led naturally to EXAFS studies of dopants in semiconductors. Indeed, a system very similar to that studied here, S implanted in GaAs, was the subject of a fluorescence EXAFS study more than eight years ago.[15] This then results in the question: Why has Si in GaAs not been investigated until only very recently?[10]

B. Defining measurement difficulties from Si-doped GaAs

(i) Unlike S in GaAs, Si is amphoteric. Therefore, a reliable interpretation of x-ray-absorption data in which Si in GaAs is suspected of occupying *both* Ga and As sites necessarily involves two separate model systems, one in which Si occupies *only* Ga sites and one where it occupies *only* As sites. The former is readily available because low concentrations of Si almost exclusively substitute for Ga in donor sites on GaAs(100). The latter system, however, requires different sample preparation.

(ii) Even if both model systems are available, the first-neighbor Si-Ga and Si-As bond lengths, and the backscattering amplitudes of the Ga and As neighbors (which differ in Z by only 2) are essentially identical. This means that the individual EXAFS from Si *coexisting* in two different sites would be difficult, if not impossible, to identify or separate.

(iii) Samples called highly doped from the standpoint of semiconductor technology are still very dilute in x-ray-absorption measurements. For example, a Si dopant concentration of 5×10^{18} cm^{-3}—which is where electrical deactivation in GaAs becomes important—corresponds to about 100 ppm. In order to obtain reference data from a fully activated sample, i.e., one without defects leading to electrical deactivation, systems of still lower concentration need to be studied. The sample with the lowest concentration studied in this work is about 30 ppm. From the effective sampling depth in these measurements of about 0.15 μm (see below), this corresponds to a signal of only ~ 0.03 monolayers of Si.

(iv) The Si K edge at 1.84 keV cannot be studied with standard x-ray monochromator crystals like Ge(111) because their $2d$ spacing is too small. Instead, InSb(111) crystals must be used. The relatively poorer thermal properties of InSb (Ref. 16) imply that temperature variations in the first monochromator crystal due to unavoidable changes in input beam intensity—such as those arising from the large range of scanned Bragg angles, the large absorption features of beamline optical elements, and the finite synchrotron beam lifetimes—are not possi-

ble to control. These temperature variations affect the reproducibility of the output beam energy,[17] position, and intensity on the sample, which is a particularly important factor when averaging multiple scans from low concentration samples.

(v) The Si $K\alpha$ signal is not only very weak compared with the intensity of host Ga and As $L\alpha$ fluorescence, but its energy at 1.74 keV is close to that of the background $L\alpha$ fluorescence at about 1.1 and 1.3 keV, respectively. Considering the limited dynamic range of solid-state detectors, the signal becomes even more difficult to discriminate from the background in this system.[18]

C. Overcoming measurement difficulties

In the order of difficulties raised in Sec. II B:

(i) Molecular-beam-epitaxy (MBE) grown samples of GaAs can be prepared with Si predominantly occupying As sites if low Si dopant concentrations are substrates oriented along the (311)A direction are used.[19] (The notation A here refers to the Ga atoms in an AB compound such as GaAs.) On the (311)A surface,[20] there are a majority of Ga atoms, so epitaxial deposition of Si onto this surface favors occupation of the majority of correspondingly available As sites.

(ii) Since EXAFS cannot distinguish between Si_{Ga} and Si_{As} sites, we focus on that part of the x-ray-absorption data that is sensitive to differences in the electronic rather than the geometric structure, i.e., the NEXAFS region. High energy resolution is essential for doing this (see below).

(iii) and (iv) To obtain sufficient statistics from low concentration samples, high beam intensities and averaging of multiple scans are used. Reproducible scans are obtained as a result of the highly stable beam on the sample. These considerations apply not only to the NEXAFS regime for identifying Si_{Ga} and Si_{As} sites, but also to the EXAFS region for investigating the formation of Si dimers and clusters. The following various design features of the beamline[21] on which the x-ray-absorption experiments were conducted allow these goals to be realized.

A Pt-coated premirror located upstream of the monochromator acts as a low-pass filter, taking out the high-energy part of the white synchrotron beam. Its cutoff energy can be changed by varying the angle of incidence on the mirror, thereby considerably reducing the heat load on the first of two monochromator crystals. (A side effect is that higher harmonics are essentially eliminated.) A design for a strain-free thermal coupling of the first monochromator crystal to a temperature-controlled heat sink is also very effective in providing temperature stability, and therefore reproducible output beam energy, position, and intensity.

The monochromator is located upstream of the bent toroidal focusing mirror, thereby removing the otherwise encountered adverse effects on energy resolution.

A servo-feedback system driving a solenoid on the second monochromator crystal provides very fine vertical positional stabilization of the beam on the sample.

A large collection angle by the focusing mirror provides a high intensity output beam.

Figure 1 illustrates some of the inherent difficulties associated with a Si K-edge absorption measurement and the success of the above beamline features in eliminating or minimizing their contributions in the data. While measurement difficulties are more demanding for dilute samples, we illustrate the effectiveness of the final result using a bulk amorphous silicon sample because there only a single first-neighbor shell, i.e., a single frequency, is observed (EXAFS from higher-neighbor shells, which would complicate the spectrum, is canceled due to static disorder). The incident beam intensity I_0 and the absorption I (monitored here by total electron yield detection) are seen to exhibit considerable structure. The most prominent features are a large glitch at $\sim$2030 eV from Bragg scattering in the InSb(111) monochromator crystal and the Pt $M_{4,5}$ absorption edges at $\gtrsim$2100 eV from the Pt coatings of the premirror and focusing mirror. However, normalizing the data by dividing I by I_0, see bottom of Fig. 1, completely cancels these structures and clearly brings out the single oscillation of the absorption coefficient arising from the nearest-neighbor scattering in a-Si.

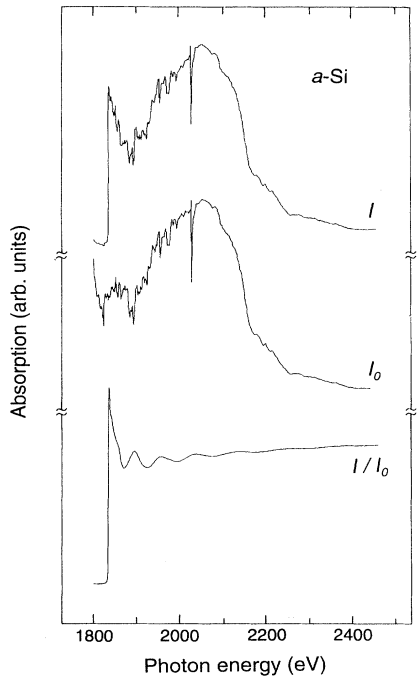

FIG. 1. Si K-edge x-ray-absorption spectrum from bulk amorphous silicon, illustrating data normalization. Dividing the x-ray-absorption intensity, I, by the incident beam intensity, I_0, removes extraneous structures due to beam instabilities, monochromator crystal glitches, and Pt $M_{4,5}$ absorption edges from Pt-coated mirrors in the beamline. Normalized data exhibit a single EXAFS frequency characteristic of a-Si.

(v) Using a seven-element fluorescence detector with individual, parallel signal paths improves the dynamic range, while a high-pass Be filter positioned between the sample and the detectors improves discrimination between the Si $K\alpha$ signal and the Ga and As $L\alpha$ background. Filtering relies on the fact that the Be mass absorption coefficients μ_{Be}(Ga) and μ_{Be}(As) at the corre-

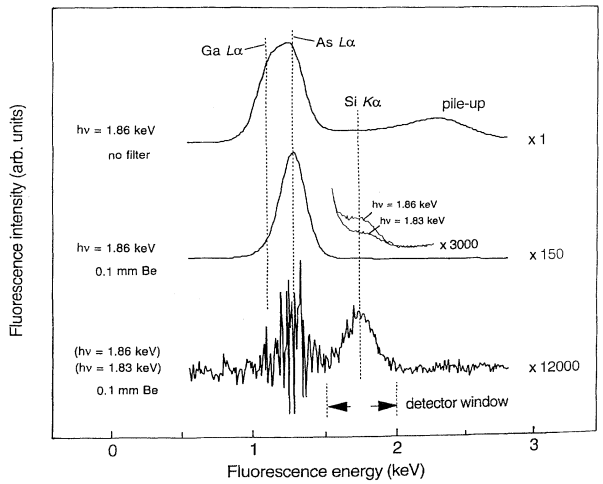

FIG. 2. Fluorescence spectra from a GaAs(100) sample doped with 1.8×10^{18} cm^{-3} Si, illustrating the optimization of Si $K\alpha$ signal detection from the Ga and As $L\alpha$ background. Upper trace: No Be filter between sample and fluorescence detector; incident x-ray energy just above 1.84-keV Si K absorption edge. Middle trace: As in the upper trace, but with a Be filter. Note scale factors. Inset shows amplified spectra above and below the Si K edge in the region of Si $K\alpha$ fluorescence. Lower trace: Result of taking the difference between a full range of middle spectra measured above and below the Si K edge. Note the emergence of Si $K\alpha$ fluorescence from the background.

sponding Ga and As fluorescence energies are somewhat larger than μ_{Be}(Si) at the slightly higher energy of the Si fluorescence. Since the Be absorption of photons with energy E is $\exp[-\mu_{Be}(E)\rho_{Be}t_{Be}]$, where ρ_{Be} is the Be density and t_{Be} is the filter thickness, the improvement in signal-to-background ratio S/B is essentially $\exp[[\mu_{Be}(\text{Ga or As})-\mu_{Be}(\text{Si})]\rho_{Be}t_{Be}]$. We have optimized S/B, i.e., kept the Si signal at a reasonable counting rate, by using an *in vacuo* filter wheel containing Be filters of different thickness in the range 0.01–0.5 mm. Best results were obtained for $t_{Be}=0.1$ mm, which gives a S/B improvement by a factor of >500 for the Ga fluorescence, >20 for the As fluorescence, and about >40 overall.

Figure 2 illustrates the effect of this filtering on the fluorescence spectrum from a low-concentration sample (<40 ppm) taken with an incident photon energy of 1.86 keV, slightly above the Si K absorption edge at 1.84 keV. The upper trace shows no visible sign of Si $K\alpha$ fluorescence because it is completely buried under the As fluorescence and the pile-up peak resulting from the limited temporal resolution of the detector. Introducing a 0.1-mm-thick Be filter, see the middle trace, strongly suppresses the Ga and, to a lesser extent, the As $L\alpha$ fluorescence. The barely observable Si $K\alpha$ signal is better seen in the comparison between spectra taken just above ($h\nu=1.86$ keV) and just below ($h\nu=1.83$ keV) the Si K edge; see the amplified region in the middle panel. The lower trace shows the corresponding difference spectrum with the Ga and As $L\alpha$ background effectively removed. The Si $K\alpha$ signal is now clearly visible. The energy discriminators following the main amplifiers are set to the energy window shown in the figure.

D. Sample preparation and measurement conditions

The samples were grown by molecular-beam epitaxy (MBE) on both (100)- and (311)A-oriented GaAs substrates at temperatures of 930 K in a chamber at base pressures of $\lesssim10^{-12}$ Torr. Si evaporation rates ranged between 0.1–0.001 μm/h to produce Si:GaAs-layer thicknesses of 2 μm. Samples were prepared at four different Si concentration regimes: below, at, above, and well above the nominal concentration of $\sim5\times10^{18}$ cm^{-3} where the onset of electrical activation is observed.[4] Hall measurements at 4.2, 77, and 300 K were performed in a van der Pauw geometry with a magnetic field of 960 G and a sample current of 100 μA. Ohmic contacts were made by depositing 0.5-mm dots of In on 4×4 mm^2 samples and annealing in forming gas at 750 K for 15 min.

The x-ray-absorption measurements were conducted on the AT&T Bell Laboratories X15B beamline[21] at the National Synchrotron Light Source. EXAFS data were taken from the two highest Si concentration samples at <60 K to minimize thermal disorder effects (Debye-Waller-like broadening).[11] The NEXAFS data, which are insensitive to such effects, were obtained from samples at room temperature. All of the samples studied showed trace amounts (typically <10 ppm) of SiO_2 which could not be removed by chemical etching or ion sputtering. This SiO_2 signal, well identified by a sharp peak about 8 eV above the Si K edge[22] and well outside the region of interest in this work, was subtracted from all the NEXAFS data shown. Fluorescence measurements were performed with the detector perpendicular to the incident x radiation, i.e., along the horizontal polarization direction of the beam, in order to minimize background Compton scattering. The samples were oriented to 45° with respect to the axes of the detector and the incident beam. In this geometry, and taking into account the absorption length of ~5000 Å for ~2-keV radiation in GaAs, the effective sampling depth probed in these measurements is approximately 1500 Å.

III. RESULTS AND DISCUSSION

A. NEXAFS: Si_{Ga} vs Si_{As} monomers

In Fig. 3 we show the Si K-edge NEXAFS data from the Si-doped GaAs(100) and GaAs(311)A samples at four different dopant concentrations labeled "low" (L), "medium" (M), "high" (H), and "very high" (VH). The normalization factors indicated at the right for each spectrum are given relative to the absolute Si atom concentration in the VH-(100) sample, 4.9×10^{19} cm^{-3}. This value was determined by assuming that the L-(100) sample is fully electrically active, i.e., the measured free-carrier (electron) concentration of that sample, 1.8×10^{18} cm^{-3}, is taken to be equal to the concentration of Si atoms occupying Ga sites, [Si_{Ga}]. [Previous determinations of total Si concentrations in the "low" to "medium" regime

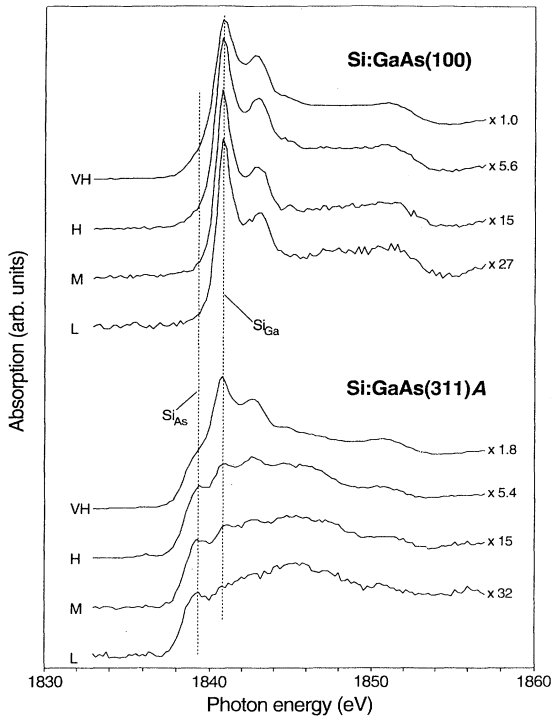

FIG. 3. Si K-edge NEXAFS data from (100)- and (311)A-oriented GaAs substrates as a function of Si dopant concentrations, labeled low (L), medium (M), high (H), and very high (VH). X-ray-absorption edge jumps, which are directly proportional to [Si], are normalized to the VH-(100) spectrum, with scaling factors indicated. Broken vertical lines identify peak absorption positions for Si occupying Ga and As sites. As [Si] increases, the occupation of opposite sites in both types of substrates is apparent.

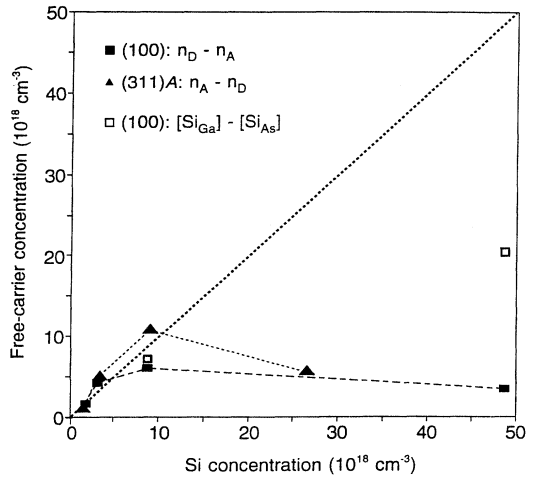

FIG. 4. Concentrations of free electrons $(n_D - n_A)$ in Si:GaAs(100) samples, filled squares, and free holes $(n_A - n_D)$ in GaAs(311)A samples, filled triangles, plotted as a function of Si concentration. The bold dashed line is an ideal case of one free carrier per Si. The lighter dashed lines are a guide to eye and reflect actual trends, showing electrical deactivation with increasing [Si]. The open squares represent what free-carrier concentrations would be in H- and VH-(100) samples if autocompensation was the only deactivating mechanism. The discrepancy between open and filled squares demonstrates that autocompensation alone cannot explain electrical deactivation at high Si doping levels in GaAs(100).

using secondary-ion mass spectroscopy (SIMS) support this procedure.] The Si concentrations in the other (100) samples were then proportionately scaled to their edge jumps measured >30 eV above the edge (outside the energy range shown in the figure) where their x-ray-absorption intensities are structureless, i.e., atomiclike. The same normalization was applied to the GaAs(311)A samples, only there the free-carrier (hole) concentration of 1.5×10^{18} cm^{-3} in the L-(311) sample is assumed to be equal to the concentration of Si atoms occupying As sites, [Si_{As}].

In Fig. 4 we plot the measured free-carrier concentrations (filled squares for electrons, filled triangles for holes) versus the corresponding Si atom concentrations from Fig. 3. The dashed line with unit slope represents the hypothetical condition in which every Si atom, regardless of concentration, is assumed to provide a single free carrier. The actual free-carrier concentrations measured for the (100) samples are seen to start saturating at [Si] $\simeq 5\times10^{18}$ cm^{-3}, consistent with earlier findings.[4,23–25] Electrical saturation for our (311)A samples occurs at about twice that amount [it is possible, however, to obtain higher carrier concentrations from (311)A samples by adjusting growth parameters].[26,27] Above these Si concentrations, the number of free carriers decreases even further. It is clear from Fig. 4 that the L, M, H, and VH concentrations in the samples studied cover the relevant region below and well above the points where electrical deactivation is first observed.

Returning to the data in Fig. 3, two characteristic features are immediately obvious for distinguishing between the L-(100) and L-(311)A spectra. First, the energy position of the absorption edge for the (311)A sample is about 1.8 eV lower than that for the (100) sample. Second, the (100) spectrum exhibits a relatively sharp absorption peak at threshold. (This peak is often called a white line, a historical reminder of the time when x rays were detected with photographic film and intense absorption lines appeared white in the film negative.)

Understanding these two features in the NEXAFS data is straightforward and explained using Fig. 5, where Si K-absorption edge data for Si in different chemical environments are compared. The L-(100) sample represents a system in which Si almost exclusively occupies Ga donor sites. In such an environment, labeled Si_{Ga}, the Si atom is positively ionized, so its K absorption energy is higher in energy than it would be as a purely neutral species in bulk Si, labeled Si_{Si}. A similar system where little charge exchange is expected is a low concentration (3%) of Si in a Ge host lattice, labeled Si_{Ge}. The origin of the absorption-energy shifts as a function of charge transfer to neighboring atoms is entirely analogous to the initial state chemical shifts of the Si 1s binding energy seen in x-ray photoemission measurements. The main difference

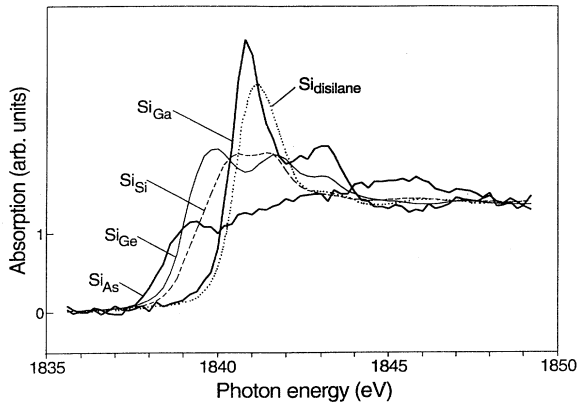

FIG. 5. Comparison of the Si K-edge absorption data for Si in five different chemical environments. All spectra have been normalized to a common edge jump, indicated by the unit tick mark on the ordinate. The notation, coordination, and corresponding samples are: Si_{Ga}=Si in Ga sites, bonded to As, from low (L) concentration Si in GaAs(100); Si_{As}=Si in As sites, bonded to Ga, from low (L) concentrations Si in GaAs(311)A; Si_{Si}=Si in Si sites, bonded to Si, from crystalline Si; Si_{Ge}=Si in Ge sites, bonded to Ge, from 3% Si in Ge; $Si_{disilane}$=Si bonded to Si and H in condensed Si_2H_6 (at 77 K). In the first four systems, the K absorption edge shifts monotonically towards higher energy with increasing transfer of charge from Si to its nearest neighbors. Comparison between the data from c-Si and Si_2H_6, both of which contain Si-Si bonding, illustrates how sensitive the unfilled Si $3p^*$ states are to the chemical environment.

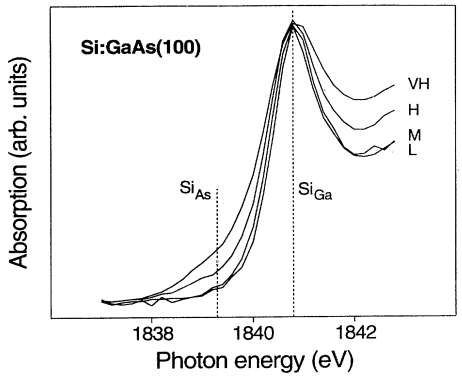

FIG. 6. Expanded Si K-edge NEXAFS spectra from Si-doped GaAs(100) samples as a function of Si concentration. Data have been normalized at the peak intensity of the white line, corresponding to the peak absorption of Si in Ga sites, to make additional intensity in the ~1839-eV region, corresponding to absorption of Si in As sites, more apparent for H- and VH-(100) samples.

between the photoemission and photoabsorption processes, however, is that in the former, the 1s core electron is photoexcited into a dipole-allowed, high-lying, structureless continuum state, whereas in the latter, that state is a low-energy unfilled level lying just above threshold. Such a level resides in, and therefore reflects, the structure of the unoccupied density of dipole-allowed states in the presence of a core hole. Now for the case of a Si K edge, the unfilled level into which the 1s electron is excited is derived largely from antibonding Si $3p^*$ states. The donor Si_{Ga} atoms are ionized, so their $3p^*$ states are more localized, or narrow, relative to the corresponding unoccupied $3p^*$ states of the Si_{Si} or Si_{Ge} atoms. This explains why the NEXAFS data from Si_{Ga} atoms exhibit a white line. [A much more intense and narrow white line is observed in the NEXAFS data from SiO_2 (Ref. 22) because the Si_O atoms are even more positively ionized, and so the $3p^*$ states are even more localized.] Analogous reasoning explains why the absorption edge in the L-(311)A sample, which almost exclusively contains negatively charged Si_{As} atoms occupying acceptor sites, exhibits no white line and is shifted to a lower energy relative to the neutral Si_{Si} species.

We now use these two features in the lowest concentration samples to identify the existence and determine the relative amounts of the Si_{Ga} and Si_{As} species as a function of increasing Si dopant concentration. In Fig. 3 we have indicated with broken vertical lines the positions of peak absorption for Si occupying the corresponding Ga and As sites at 1840.8 and 1839.8 eV, respectively. It is obvious in the (311)A spectra that the M, H, and VH concentrations exhibit an increasingly pronounced white-line structure characteristic of Si_{Ga}. Similarly, in the H- and VH-(100) spectra a growing pre-edge structure occurs at the position of the Si_{As} edge, thus pointing to the existence of these species as well. Casual inspection of Fig 3 does not readily reveal these latter species, however, so the edge region has been magnified in Fig. 6. The normalization to the peak of the white line makes not only the population of Si_{As} atoms more obvious, but it also clearly shows that the L and M spectra look very similar, indicating that in these samples very few opposite-site Si atoms are present and that the samples are fully activated. In effect, this result independently proves that the L-(100) NEXAFS data represent the pure Si_{Ga} species in GaAs.

In order to quantify the above observations for the H- and VH-GaAs(100) samples, we have least-square fit the NEXAFS data using the L-(100) and L-(311) samples as models for the pure Si_{Ga} and pure Si_{As} species, respectively. The fits were constrained over two energy regions: below the white line, 1835–1839.3 eV, where the spectra are most sensitive for determining the existence of Si_{As}, and well above the white line, 1860–1865 eV, where the data are relatively structureless for keeping the total edge jump constant. Note that this fitting approach provides an *upper limit* to the concentration of Si_{As} sites, since it implicitly assumes that Si_{Ga} and Si_{As} are the *only* constituents in a H or VH sample. Other possible defects—whose contributions to the observed NEXAFS data have not been included—would obviously decrease the concentrations of both Si_{Ga} and Si_{As} in the fits.

The results of the fits are shown in Fig. 7. From the concentrations of $[Si_{As}]$=12% and 29% determined in the fits for the H-(100) and VH-(100) samples, respectively, the free-carrier concentrations can be calculated as-

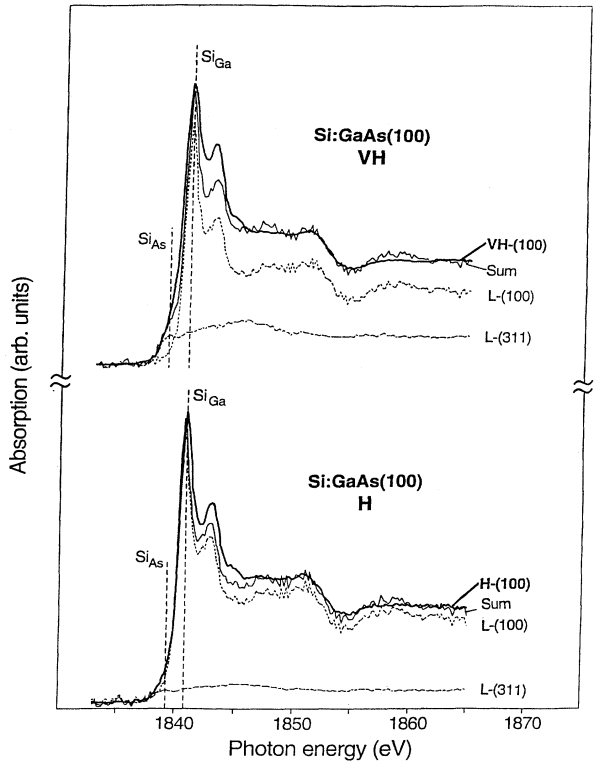

FIG. 7. Determining the upper-limit concentration of Si occupying As sites in VH and H samples of GaAs(100). Assuming that Si occupies only As and Ga sites, represented by corresponding L-(311) *A* and L-(100) data (dashed lines), the VH-(100) and H-(100) data (bold lines) are fitted between 1834–1839.3 eV. The result of the fit (solid line, labeled "Sum") gives $[Si_{As}]/([Si_{As}]+[Si_{Ga}])=29\%$ and 12% for VH and H samples, respectively. Note misfit with data between 1839.3–1845 eV in both cases (albeit smaller for the H sample), indicating Si must also be present in other than As and Ga sites.

suming that autocompensation is the exclusive deactivation mechanism. The so-calculated electrical activities, namely, $88\%[Si_{Ga}]-12\%[Si_{As}]=76\%$ and $71\%[Si_{Ga}]-29\%[Si_{As}]=42\%$, are indicated in Fig. 4 by open squares. These results carry the following implications.

(i) In Fig. 7, there are regions of obvious misfit above the Si_{Ga} white line. There is also misfit below the Si_{Ga} white line in the case of the VH-(100) sample. These observations directly indicate that *in both* H and VH samples, a Si species other than Si_{Ga} and Si_{As} *must* be present.

(ii) In addition to and consistent with the misfitted data, the autocompensation mechanism alone is *insufficient* for explaining the observed electrical activity. From Fig. 4 for the VH-(100) sample, the actual measured fraction of electrically active Si atoms is only 7% of the idealized free-carrier value. This means that at least $(42\%-7\%)/(100\%-7\%)=38\%$ of the observed electrical activity remains unexplained by autocompensation. This value is not only substantial, but because the concentration of Si in As sites has been overestimated, it actually represents a lower limit. Using a more realistic value of $[Si_{As}]$, i.e., one which also includes Si in environments other than Si_{Ga} and Si_{As}, we estimate that in this sample about *half* of the observed electrical deactivation is unexplained by autocompensation. For the H-(100) sample, which represents more commonly used dopant concentrations, we arrive at a similar conclusion. Specifically, we find from Fig. 4 that at least $(76\%-65\%)/(100\%-65\%)=31\%$ of the observed activity remains unexplained.

We are now left with the question of which species accounts for the remainder of the electrical deactivation. A number of other point defects have been proposed in Si-doped GaAs, but experimental evidence for their importance is generally lacking. These include the following:

(a) Si dimers, $(Si_{Ga}-Si_{As})^0$. These electrically neutral defects are calculated to be energetically favorable[2,28] and have been identified by using LVM spectroscopy.[6] A quantitative estimate of their concentration, however, is not possible to calculate for samples prepared under nonequilibrium conditions, e.g., those grown in this work with MBE. Furthermore, the LVM data[6] cannot reliably determine dimer concentrations for reasons briefly mentioned in the Introduction and discussed in Sec. IV.

(b) Si clusters, Si_n, where $n>2$. Large clusters (precipitates) might be expected to be the most important type of defect in highly doped samples such as H- and VH-(100), since their concentrations are above the solubility limit of $\gtrsim 7\times10^{18}$ cm^{-3} for melt-grown *n*-type GaAs at 900 K (Refs. 28 and 29). However, transmission electron microscopy (TEM) studies of these particular samples[30] show no evidence of clusters within the <0.2-μm region probed in our x-ray-absorption measurements. Given the detection limit for TEM of ~10 Å, this means that any clusters, if present, do not contain more than ~25 Si atoms.[22] The lack of Si precipitation at doping concentrations well exceeding the calculated solubility limit is another example[31] of how equilibrium (thermodynamic) concepts are inapplicable to nonequilibrium (kinetic) processes such as MBE.

(c) Other defects, such as Si vacancy complexes, $(Si_{Ga}-V_{Ga})^{2-}$, Ga vacancies, $(V_{Ga})^{3-}$, and *DX* centers. $(Si_{Ga})^-$. All of these can contribute to a decrease in electrical activity in *n*-type GaAs, since they act as acceptors.

The point defects outlined above unfortunately cannot be quantified, or even reliably identified, in our NEXAFS data for two reasons. First, and most important, is that an accurate model system for any one of them is unavailable: there is no known experimental means for preparing a sample containing only a single type of defect in categories (a)–(c), and there is no theoretical approach for calculating its NEXAFS spectrum that would be viewed sufficiently reliable for quantitative analysis. (Recall that NEXAFS reflects the electronic-chemical structure of the absorbing atom in the presence of a core hole, so the model system must be identical, not just similar, to the one under investigation. Thus, for example, the NEXAFS from a $(Si_{Ga}-Si_{As})$ dimer or a Si_n cluster cannot be approximated by that from Si_2H_6 or *c*-Si because of the detailed differences in the unfilled Si $3p^*$ states.) Second, even if such model systems did somehow become

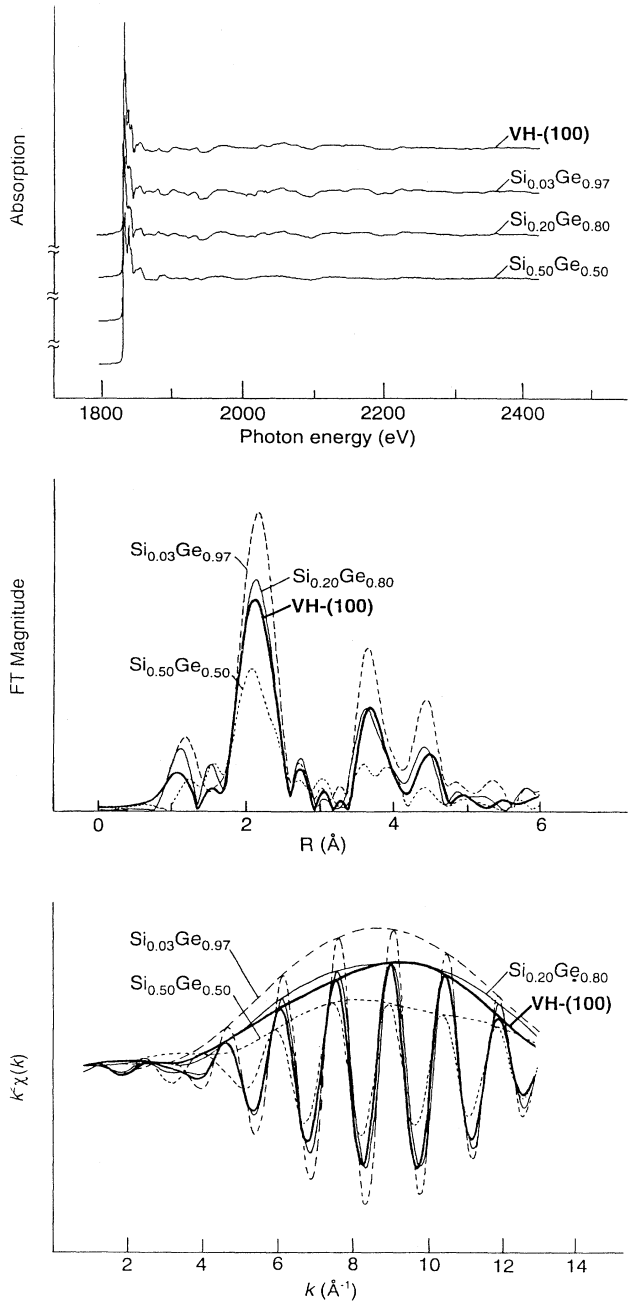

FIG. 8. Top panel: Raw Si *K*-edge EXAFS data from the VH sample of Si:GaAs(100) and three Si-Ge alloys of varying composition. Middle panel: Fourier transforms of edge-truncated, background-subtracted, and k^2-multiplied data from samples in the top panel. First-, second-, and third-shell peaks, uncorrected for phase shift, appear at ~2.1, 3.7, and 4.5 Å, respectively. Smaller peaks at ~1.2 and 2.8 Å are due to residual background and truncation. Bottom panel: Filtered first-shell EXAFS data, obtained by placing a window around the first-neighbor peak in Fourier-transformed data (1.6–2.6 Å) and then backtransforming into k space. Amplitude functions enveloping oscillatory EXAFS data are also shown. In the middle and lower panels, note the strong similarity between data from VH-(100) and $S_{0.20}Ge_{0.80}$ samples, indicative of very similar local structural environments.

available, the region between the two absorption edges of the Si_{As} and Si_{Ga} species—where the contribution of other defects is expected to be most important—is simply too narrow for a meaningful analysis.

Despite these limitations, it is important to point out that our claim of having experimentally determined an upper limit for $[Si_{As}]$—and by extension, of having demonstrated the inadequacy of autocompensation for fully explaining the observed electrical deactivation—still remains valid. The reason for this is that the white-line region of the Si_{Ga} species, which we have argued must contain contributions from the other defects [(a)–(c)] in order to explain the misfit of the NEXAFS data in Fig. 7, is not used at all in the fits. Therefore, the principal conclusion to be drawn from the above discussion is that the near-edge region of the absorption spectrum is not appropriate for determining the type and amount of *other* point defects in highly Si-doped GaAs. Another approach is required.

B. EXAFS: Si dimers and clusters

While the near-edge (NEXAFS) region requires identical model systems for accurate assignments of the absorbing species, the extended (EXAFS) region is more forgiving because it reflects the scattering of photoelectron waves from core-dominated, chemically insensitive potentials.[11] Using Si:Ge model systems to approximate Si:GaAs, which is the approach we shall take, is therefore well justified because the core potential of Ge is so similar to that of Ga or As. With this in mind, we show how it is possible to obtain geometric structural information from EXAFS data of point defects in Si:GaAs.

The top panel of Fig. 8 shows the raw absorption spectrum from the VH-(100) sample, along with comparable spectra from three $Si_xGe_{1-x}(100)$ alloys with $x=3\%$, 20%, and 50%. To isolate the EXAFS, $\chi(k)$, the data are analyzed following standard procedures,[11] namely, truncating above the edge, removing a smooth background, and converting from photoelectron energy space into photoelectron momentum (k) space, weighed by k^2. The raw, background-subtracted data are then Fourier transformed into distance (R) space to isolate the different nearest-neighbor shells around the absorbing Si atom. The result, see middle panel of Fig. 8, clearly reveals the first three shells at approximate distances (uncorrected for scattering phase shifts) of 2.1, 3.6, and 4.4 Å (the smaller peaks in the transform correspond to a combination of residual background, noise, and truncation errors). We isolate the nearest-neighbor EXAFS from that of the higher shells by placing a filter around the first-neighbor peak and backtransforming into k space. The filtered first-shell data for the VH-(100) and Si_xGe_{1-x} samples are shown in the bottom panel of Fig. 8, along with the corresponding amplitude functions $A(k)$ that envelope the oscillatory EXAFS.

Two important results are obvious from inspection of the filtered data: The peak intensities of $A(k)$ for the Si-Ge alloys decrease with increasing Si content, and the VH-(100) data are very similar to that of $Si_{0.20}Ge_{0.80}$. The first result can be understood by recalling that the

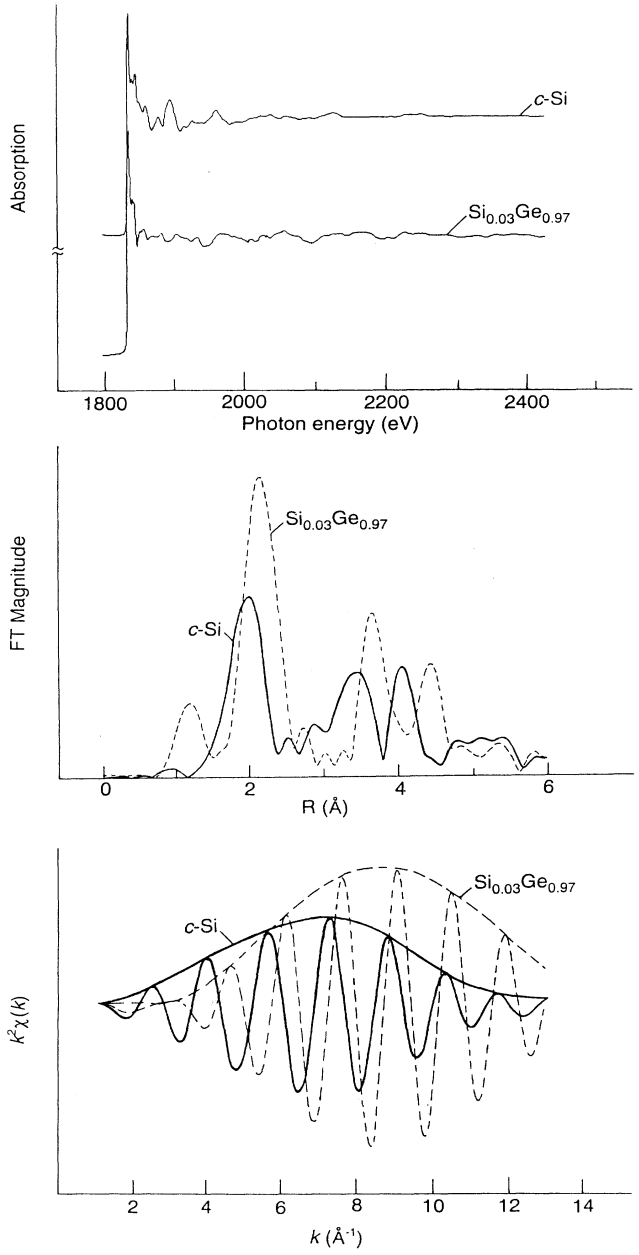

FIG. 9. Same as in Fig. 8, but for crystalline Si compared with a $Si_{0.03}Ge_{0.97}$ alloy. Note that the different Si-Si vs Si-Ge first-shell bond lengths and Si vs Ge first-shell neighbors around Si lead to readily distinguishable differences in the corresponding EXAFS data.

bond length between Si-Si is somewhat shorter than between Si-Ge, and that the backscattering amplitudes for Si and Ge are different as well. This contrast is apparent by comparing identically analyzed EXAFS data from *c*-Si with that from $Si_{0.03}Ge_{0.97}$, see Fig. 9. The different phases and amplitudes of photoelectron waves backscattered from Si and from Ge atoms in $Si_{0.20}Ge_{0.80}$ lead to destructive interference, resulting in a reduction of overall amplitude proportional to the coordination number of Si atoms in the first-neighbor shell.

The second result is understood by the fact that Si and Ge are perfectly miscible. This means that the distribution of Si-Si, Si-Ge, and Ge-Ge bonds is purely statistical and that the average coordination number of first-neighbor Ge and Si atoms, N_{Ge} and N_{Si}, is straightforward to determine. In $Si_{0.03}Ge_{0.97}$, for example, $N_{Ge}=4(0.97)=3.88$ and $N_{Si}=4(0.03)=0.12$; as expected a dilute concentration of Si in Ge is surrounded by essentially four Ge and no Si first-nearest neighbor (this is the reason for using that sample to represent Si_{Ge} in Fig. 5). Similarly, in $Si_{0.20}Ge_{0.80}$, on average,[32] $N_{Ge}=3.2$ and $N_{Si}=0.8$, and in $Si_{0.50}Ge_{0.50}$, $N_{Ge}=N_{Si}=2$. Recalling that Ge and GaAs have nearly identical bond lengths and backscattering amplitudes, the second result therefore implies that the VH-(100) Si:GaAs sample has the same average Si-Si coordination as a random distribution of 20% Si. A more rigorous evaluation of the data using a least-squares fitting routine[11] arrives at the same conclusion, namely, $N_{Si}=0.8\pm0.2$.

This average value of N_{Si} does not tell us to what extent the Si-Si coordination is due to dimers or clusters, i.e., it gives no direct information about the distribution of n in Si_n cluster sizes. Figure 10 schematically illustrates this point for the case of eight Si atoms that are allowed to form different combinations of monomers ($n=1$), dimers ($n=2$), and clusters ($n>2$). Assuming, for simplicity, that in this example $N_{Si}=1$, there are several distributions shown in Fig. 10 that are possible.

We now extend this reasoning to the case of the VH-(100) sample by considering three limiting cases: only

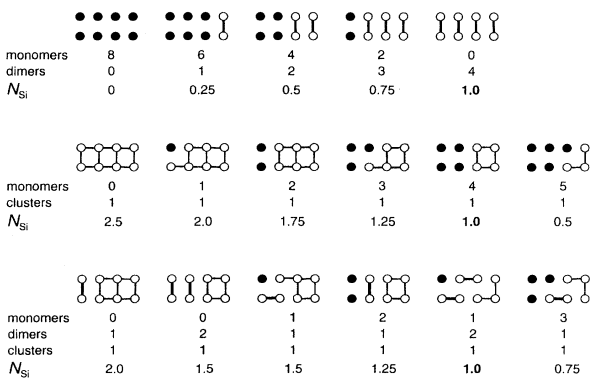

FIG. 10. Schematic picture of different concentrations and distributions of eight Si atoms in a GaAs host lattice. Three generic Si-atom concentrations, Si_n, are shown: monomers ($n=1$), filled circles, with no Si neighbors; dimers ($n=2$), open circles and one bold bond, each with one Si neighbor; and clusters ($n>2$), open circles and no bold bonds, containing at least one Si atom with more than one Si neighbor. Three types of distributions are shown: only monomers and dimers; only monomers and clusters; and monomers, dimers, and clusters. The average Si-atom coordination, N_{Si}, for a particular distribution is the number of Si neighbors for each Si atom divided by the total number of Si atoms, 8. Not all possible distributions are shown. An EXAFS determination of $N_{Si}=1.0$, for example, significantly limits the choice of possible distributions but requires additional information to make further distinctions.

monomers and dimers, only monomers and clusters, and a random mixture. For the first distribution to be consistent with our measured value of $N_{Si}=0.8$ requires that 80% of the Si atoms are dimers and 20% are monomers. To arrive at our measured value of 7% electrical activity, and assuming that no other point defect listed in category (c) above plays a significant role, the monomers would be divided up into $\sim 14\%$ $Si_{Ga}$and $\sim 7\%$ Si_{As}. We believe this distribution can be ruled out based on the following arguments. First, the fit of the NEXAFS spectrum in the region of the Si_{As} species (see Fig. 7) is excellent, giving a limit of $[Si_{As}] \leq 29\%$. If 80% of the doped Si atoms were in $(Si_{Ga}-Si_{As})$ dimers, then that same NEXAFS region would have to accommodate 7% of the Si_{As} monomers plus an additional 40% of dimerized Si_{As} whose NEXAFS data would have to be energetically unshifted (or nearly so) from the monomer but reduced in amplitude by an upper value of $(29\%-7\%)/40\%=55\%$. This seems implausible. Second, according to the Fourier-transformed EXAFS data in Fig. 8, the second- and third-neighbor shells in the VH-(100) sample closely resemble those in $Si_{0.20}Ge_{0.80}$. Both are clearly reduced in intensity relative to those in $Si_{0.03}Ge_{0.97}$ because of the Si scattering, as discussed above. If only dimers and monomers were present in the VH-(100) sample, these shells would not be significantly affected. Third, the diffusion coefficient for Si dimers is about two orders of magnitude larger than for monomers[33] at 900 K, making it unlikely that the dimers, after having been formed, would not diffuse and form larger clusters.

If we assume a distribution of only monomers and clusters, all the clusters would have to be smaller in size that the detection limit of TEM, ~ 10 Å. According to an analysis given in Ref. 22, such clusters would have an average Si-Si coordination number N_{Si} of at least 2.3. This means that at most $(0.8/2.3)=35\%$ of the Si atoms could be associated with those clusters. As argued above, at least 36% would then be Si_{Ga} monomers and 29% would be Si_{As} monomers. This latter value for the required minimum concentration for Si_{As} is right at the upper limit established by NEXAFS, so on the basis of our data alone we cannot completely rule out this assumed distribution. In order to do that, we must rely on LVM results[6] from similarly doped samples, which show clear evidence for $(Si_{Ga}-Si_{As})$ dimers. (Of course, we could have used these LVM results in the first place to reject the assumption of no dimers.)

Finally, a random distribution of 20% Si atoms in Ge produces $(0.80)^4=41\%$ monomers and predicts $(0.80)^6\times 4(0.20)=21\%$ of the Si atoms to be in dimers. This leaves 38% in clusters, whose N_{Si} value averaged over all sizes and shapes must be less than $(0.8-0.21)/0.38=1.55$. Such a low Si coordination implies[22] very small cluster sizes, in accord with the TEM results. Using the results of our Hall measurements leads to $[Si_{Ga}]=24\%$ and $[Si_{As}]=17\%$, compatible with our NEXAFS data. Finally, the prediction of both clusters and dimers in a random distribution is consistent with the effect of Si-Si scattering in the second and third shell of Si_n clusters of our EXAFS data and with the independent LVM evidence for dimers[6] from comparably Si-doped GaAs(100). This overall consistency with the $Si_{0.20}$ $Ge_{0.80}$ sample does not, of course, imply that the distribution of monomers, dimers, and clusters in the VH-(100) sample actually is or should be random, particularly since the actual Si concentrations in and the preparations of the two samples are so very different. Rather, it simply means that the composition of different Si-containing point defects produced under the particular MBE growth conditions used for preparing the VH sample turns out to resemble a distribution very similar to that found in the $S_{0.20}Ge_{0.80}$ alloy.

Having identified the dominant Si-containing point defects in the VH-(100) sample, it is tempting to see whether additional information about the other point defects in category (c), which have so far been ignored, can also be observed in our EXAFS data (recall from Sec. III A that without identical model systems it is not possible to use NEXAFS data for identifying these species). The most important of these other defects is calculated[28,29] to be $(Si_{Ga}-V_{Ga})^{2-}$, whose structure differs from that of the monomeric species primarily in the second-neighbor shell. This makes a detailed evaluation, which is already difficult due to the comparatively small concentration of such defects, even more difficult. A similar statement applies to the *DX* center, $(Si_{Ga})^-$. Added to these practical limitations is the fact that the $[V_{Ga}]^{3-}$ defect is not even accessible in a Si K-edge EXAFS measurement. It is therefore apparent that extracting further information about these minority defects is not feasible with the present data.

Finally, we turn to the H-(100) sample. Analysis of its EXAFS spectrum gives an average value of $N_{Si}\approx 0.3$, substantially lower than that for the VH-(100) sample. This is consistent with the smaller degree of misfit in the Si_{As} edge region seen in Fig. 7 and with the smaller degree of unaccounted electrical deactivation shown in Fig. 4. However, the lower concentration of Si in this sample, and the correspondingly lower concentration of Si_{As} species, makes a more quantitative assessment of other defect concentrations impractical.

IV. COMPARISON WITH OTHER MICROSCOPIC METHODS

There are numerous electronic, compositional, and transport measurements available for characterizing macroscopic properties of doped semiconductors in general, and Si-doped GaAs in particular. For studying the geometric structure of dopant-related point defects on a microscopic level, there now exist at least three experimental methods: local vibrational mode (LVM) spectroscopy, cross-sectional scanning tunneling microscopy (XSTM), and near-edge–extended x-ray-absorption fine-structure (NEXAFS and EXAFS). In this discussion, we simply refer to the latter approach as x-ray-absorption spectroscopy (XAS), and the other two as LVM and STM.

Apart from their common application interests, these methods share a number of other similarities. All three are based on well-established measurement techniques—

tunneling, ir, and x-ray absorption—which underwent a first round of major experimental advances—piezoelectric-controlled scanning, fast-Fourier spectrometers, and synchrotron radiation sources. To achieve a successful application to bulk-doped semiconductors, however, all required a second round of improvements—sample cleaving *in vacuo* to probe the bulk in cross-section, 2-MeV electron irradiation of samples to form traps which eliminate free-carrier absorption, and stabilized beam and beamline features with filtered fluorescence detection to enhance signal-to-background ratios. As a result of the additional improvements, the three techniques now also share a similar limitation to convenient accessibility because only relatively few facilities and/or institutions are currently equipped to make these specialized measurements.

Comparisons between LVM, STM, and XAS extend beyond their broad similarities. Only XAS can study as-prepared samples. The electron irradiation required for LVM has been reported to have little effect on the redistribution of Si atoms in *n*-type GaAs (Ref. 7) but to have significant effects in *p*-type GaAs.[34] The crystal cleaving required for STM may be difficult or impractical for some substrates of unfavorable size or surface orientation. Both LVM and XAS are atom specific, so only the local structures around the dopant are obtained. STM relies on different bias voltages to distinguish between different types of defects, so they need not be directly associated with the dopant atoms. For examples, in addition to the bright features in the STM images from *n*-type Si:GaAs assigned to donor Si_{Ga} atoms, dark features were also observed and attributed to Ga vacancies, $(V_{Ga})^{3-}$.[9]

This brings up the relative capabilities of detecting, identifying, and quantifying different dopant atom configurations in the three different methods. As shown in this work, XAS can observe single dopant species for $Z \geq 6$ (Ref 35) at concentrations $\lesssim 10^{18}$ cm^{-3},[36] and the same order of magnitude for dopants coexisting in other configurations (e.g., $[Si_{As}] \lesssim 0.12[Si]$ for the H-(100) sample, where $[Si] \lesssim 9 \times 10^{18}$ cm^{-3}). Different dopant configurations, at least for the first three or four most dominant species, can be readily identified empirically [e.g., Si_{Ga}, Si_{As}, and $(Si_{Ga}-Si_{As})+Si_n$]. Concentrations of single dopant species are representative and quantitative, since XAS macroscopically probes the sample >0.1 μm deep and measures edge jumps, which are directly proportional to atomic concentration via the mass absorption coefficient. Absolute concentrations of coexisting dopants are difficult to quantify, but upper limits to these concentrations are reliable because they are constrained by the magnitude of the individual edge jumps and the independently measured free carrier concentrations.

LVM detection sensitivity is comparable to XAS for Si in GaAs, although the method is generally limited to light dopant atoms relative to the host (as mentioned above, *p*-type samples also pose difficulties). Coexisting dopant configurations can be observed more easily than in XAS due to its higher-energy resolution, but identifying all the species is not always straightforward.[7,37] Moreover, while the measurement does represent a macroscopic average of the sample, its most serious limitation is correlating observed peak intensities with atom concentrations. This requires knowledge of oscillator strengths, and these are not well determined. It is therefore difficult to establish whether certain observed peaks represent dilute species with large oscillator strengths, or whether more important species with weak oscillator strengths may go unobserved.

The detection sensitivity of STM is, in principle, its greatest asset since it is the individual dopant atoms, regardless of Z, that are imaged. The ability of STM to detect coexisting dopant configurations is not possible to assess at present because the types of dopant chosen and the dopant concentrations studied thus far lead to only a single configuration. There are indications, however, which suggest there may be some difficulties. The effective spatial extent of a single dopant atom in the STM images is about 25 Å,[8,9] which presents no problem at low concentrations but which at higher doping levels leads to overlapping, smeared features[8] that could obscure minority configurations. Identifying other species may also be problematic because of ambiguities in correlating bias voltages with particular configurations. As with LVM, a limitation is determining reliable concentrations, but for different reasons. Certainly it is straightforward enough to count atoms, but if only five or so substrate layers are probed, the statistics representing possible coexisting species in lower concentrations becomes increasingly important. In this regard, the study of two-dimensional δ-doped layers would appear to be even more seriously limiting for STM because the second lateral dimension for averaging scanned images is absent. However, these systems actually present a particularly promising area for future STM studies of a different kind, because the widths of the δ layers and their changing profile with temperature in studying defect diffusion and mobility could be imaged directly.

V. CONCLUSIONS

The utility of x-ray-absorption spectroscopy—in particular NEXAFS and EXAFS—for studying point defects associated with dopants in semiconductors has been extended to include one of the most common yet challenging systems, Si-doped GaAs. A number of improvements were made to overcome inherent limitations from the GaAs background signals and the measurement technique itself. Four types of Si-related defects were identified: donor Si atoms in Ga sites, Si_{Ga}; acceptor Si atoms in As sites, Si_{As}; and a combination of neutral Si dimers within the GaAs lattice, $(Si_{Ga}-Si_{As})$, plus small (<10-Å diameter) neutral Si-atom clusters, Si_n. The relative concentrations of these configurations depended on the total Si doping level and orientation of the GaAs surface. From the upper-limit concentrations determined for the different point defects in a highly Si-doped GaAs(100) sample grown by MBE, the autocompensation mechanism was shown to account for only about half of the observed electrical deactivation. Finally, capabilities and limitations of the present microscopic approach were compared with STM and LVM spectroscopy.

ACKNOWLEDGMENTS

We thank R. Hull for the TEM micrographs of the Si-doped GaAs samples, Y.-H. Xie for the Si-Ge alloy samples, J. E. Northrup for unpublished calculations of point-defect concentrations, and our colleagues at AT&T Bell Laboratories for helpful discussions. S.S. is grateful to the Alexander-von-Humboldt Foundation for financial support. The x-ray-absorption measurements were performed at the National Synchrotron Light Source, Brookhaven National Laboratory, which is supported by the Department of Energy, Division of Materials Science and Division of Chemical Sciences.

---

*Present address: Institut für Nukleare Festkörperphysik, Forschungszentrum Karlsruhe, D-76021 Karlsruhe, Germany.

†Present address: Department of Material Science, University of Illinois at Urbana-Champaign, Urbana, IL 61801.

[1]J. S. Blakemore, *Gallium Arsenide* (AIP, New York, 1987).

[2]C. Kolm, S. A. Kulin, and B. L. Averbach, Phys. Rev. **108**, 965 (1957).

[3]H. Welker, Z. Naturforschung **7a**, 744 (1952).

[4]J. M. Whelan, J. D. Struthers, and J. A. Ditzenberger, *Proceedings of the International Conference on Semiconductor Physics, Prague, Czechoslovakia, 1960* (Academic, New York, 1961), p. 943.

[5]For a recent review, see E. F. Schubert, *Doping in III-V Semiconductors* (Cambridge University, Cambridge, 1993).

[6]J. Maguire, R. Murray, R. C. Newman, R. B. Beall, and J. J. Harris, Appl. Phys. Lett. **50**, 516 (1987).

[7]R. Murray, R. C. Newman, M. J. L. Sangster, R. B. Beall, J. J. Harris, P. J. Wright, J. Wagner, and M. Ramsteiner, J. Appl. Phys. **66**, 2589 (1989).

[8]M.-B. Johnson, O. Albrektsen, R. M. Feenstra, and H. W. M. Salemink, Appl. Phys. Lett. **63**, 2923 (1993).

[9]J. F. Zheng, X. Liu, N. Newman, E. R. Weber, D. F. Ogletree, and M. Salmeron, Phys. Rev. Lett. **72**, 1490 (1994).

[10]S. Schuppler, D. L. Adler, L. N. Pfeiffer, K. W. West, E. E. Chaban, and P. H. Citrin, Appl. Phys. Lett. **63**, 2357 (1993).

[11]P. A. Lee, P. H. Citrin, P. Eisenberger, and B. M. Kincaid, Rev. Mod. Phys. **53**, 769 (1981).

[12]See, for example, *X-ray Absorption: Principles, Applications, Techniques of EXAFS, SEXAFS, and XANES*, edited by D. C. Koningsberger and R. Prins (Wiley, New York, 1988).

[13]P. H. Citrin, P. Eisenberger, and J. E. Rowe, Phys. Rev. B **28**, 2299 (1983).

[14]Signal/background considerations, among other factors, also affect the choice of detection scheme, cf., P. H. Citrin, J. Phys. (Paris) Colloq. **47**, C8-437 (1986).

[15]F. Sette, S. J. Pearton, J. M. Poate, and J. Stöhr, Phys. Rev. Lett. **56**, 2637 (1986).

[16]A useful figure of merit is the thermal conductivity divided by the thermal expansion coefficient and the absorption coefficient. For InSb at 2000 eV, this figure is about 2.5 and 30 times lower than that for Ge and Si, respectively.

[17]Z. Hussain, E. Umbach, D. A. Shirley, J. Stöhr, and J. Feldhaus, Nucl. Instrum. Methods **195**, 115 (1982).

[18]In Ref. 15, the S $K\alpha$ signal at 2.3 keV could be discriminated from the Ga and As $L\alpha$ background by using a lower-resolution proportional counter because of the relatively higher S $K\alpha$ fluorescence energy and because of the higher S concentrations in the samples studied.

[19]W. I. Wang, E. E. Mendez, T. S. Kuan, and L. Esaki, Appl. Phys. Lett. **47**, 826 (1985).

[20]The $(311)A$ rather than $(111)A$ surfaces were used to avoid difficulties with surface polishing and MBE preparation.

[21]A. A. MacDowell, T. Hashizume, and P. H. Citrin, Rev. Sci. Instrum. **60**, 1901 (1989).

[22]S. Schuppler, S. L. Friedman, M. A. Marcus, D. L. Adler, Y.-H. Xie, F. M. Ross, T. D. Harris, W. L. Brown, Y. J. Chabal, E. E. Chaban, L. E. Brus, and P. H. Citrin, Phys. Rev. Lett. **72**, 2648 (1994).

[23]K. Ploog, A. Fischer, and H. Künzel, J. Electrochem. Soc. **128**, 400 (1981).

[24]Y. G. Chai, R. Chow, and C. E. Wood, Appl. Phys. Lett. **39**, 800 (1981).

[25]J. H. Heave, P. J. Dopson, J. J. Harris, P. Dawson, and B. Joyce, Appl. Phys. A **32**, 195 (1983).

[26]T. Takamori, T. Fukunaga, J. Kobayashi, K. Ishida, and H. Nakashima, Jpn. J. Appl. Phys. **26**, 1097 (1987).

[27]K. Agawa, K. Hirakawa, N. Sakamoto, Y. Hishimoto, and T. Ikoma, Appl. Phys. Lett. **65**, 1171 (1994).

[28]J. E. Northrup and S. B. Zhang, Phys. Rev. B **47**, 6791 (1993).

[29]J. E. Northrup (private communication).

[30]R. Hull (private communication).

[31]A striking example of MBE-doped samples with concentrations exceeding the solubility limit by several orders of magnitude is Sb-doped Si, cf., H.-J. Gossmann, F. C. Unterwald, and H. S. Luftman, J. Appl. Phys. **73**, 8237 (1993).

[32]We were able to verify the stoichiometries of the Si_xGe_{1-x} alloys directly (to $\pm 5\%$) by fitting our EXAFS data with pure Si and pure Ge standards.

[33]M. E. Greiner and J. F. Gibbons, Appl. Phys. Lett. **44**, 750 (1984).

[34]M. J. Ashwin, M. R. Fahy, and R. C. Newman, J. Appl. Phys. **73**, 3574 (1993).

[35]EXAFS from atoms with $Z < 6$ is impractical because the data length above the edge is too limited (the mass absorption coefficient decays with energy too rapidly in this region). In principle, however, NEXAFS from these atoms is possible.

[36]The case of Si in GaAs is close to a worst case system in detection sensitivity for reasons discussed in Sec. II B. Lower dopant concentrations can be easily measured with XAS, e.g., $\lesssim 10^{17}$ cm^{-3} Sb in Si and $\lesssim 10^{16}$ cm^{-3} Si in C, cf., D. L. Adler, S. Schuppler, and P. H. Citrin (unpublished).

[37]H. Ono and R. C. Newman, J. Appl. Phys. **66**, 141 (1989).